Magnetostructural transition in $Gd_5Sb_{0.5}Ge_{3.5}$

A. S. Chernyshov,[1,2,*] Ya. Mudryk,[1] D. Paudyal,[1,2] V. K. Pecharsky,[1,2,†] K. A. Gschneidner, Jr.,[1,2] D. L. Schlagel,[1] and T. A. Lograsso[1]

[1]*The Ames Laboratory, U.S. Department of Energy, Iowa State University, Ames, Iowa 50011-3020, USA*

[2]*Department of Materials Science and Engineering, Iowa State University, Ames, Iowa 50011-2300, USA*

(Received 26 August 2009; revised manuscript received 13 October 2009; published 17 November 2009)

Magnetic and crystallographic properties of $Gd_5Sb_{0.5}Ge_{3.5}$ were investigated using dc magnetization, ac magnetic susceptibility, and heat capacity of an oriented single crystal, combined with temperature and magnetic field dependent x-ray powder diffraction. The compound undergoes an unusual magnetostructural transition at 40 K and a nonmagnetic second-order transition around 63 K. The detailed crystallographic study of $Gd_5Sb_{0.5}Ge_{3.5}$ shows that contrary to the $R_5(Si_xGe_{1-x})_4$ systems (R is a rare-earth metal), the structural transition occurs without shear displacements of the $^2_\infty[R_5T_4]$ slabs (T=Si, Ge, and Sb), and a substantial volume change (−0.5%) does not lead to a change in crystallographic symmetry. The first-principles electronic structure calculations show higher interslab than intraslab ferromagnetic exchange interaction indicating that Sm_5Ge_4 type of structure supports a ferromagnetic ground state in $Gd_5Sb_{0.5}Ge_{3.5}$.

DOI: 10.1103/PhysRevB.80.184416 PACS number(s): 75.20.En, 75.50.Cc, 71.20.Eh, 64.70.kd

I. INTRODUCTION

Recent investigations of magnetic and crystallographic properties of intermetallic compounds reveal substantial interest in phase transitions, where a change in the magnetic properties, usually magnetic ordering, is coupled with changes in the crystal structure. These *magnetostructural* transformations are commonly accompanied by distinct changes in the unit-cell volume, resulting in first-order phase transformations.[1–5] Such behavior is well-known in the broadly studied $R_5(Si_xGe_{1-x})_4$ systems, where R is a rare-earth metal.[6] This series of compounds has attracted considerable attention since 1997, when Pecharsky and Gschneidner discovered the giant magnetocaloric effect in the $Gd_5Si_2Ge_2$ compound.[7] The magnetostructural transitions in these alloys can be controlled by tuning chemical composition, temperature, pressure, or magnetic field parameters.[6,8–10] Numerous physical phenomena, e.g., giant magnetocaloric effect,[11,12] giant magnetostriction,[1,13] giant magnetoresistance,[14,15] spontaneous generation of voltage,[16] and various effects related to phase separation[17–21] are observed in these compounds and are all associated with first-order transitions.

It was soon realized that interesting properties can be observed not only in $R_5(Si_xGe_{1-x})_4$ systems, but the substitution of Ge by Ga,[22] Sn,[23,24] and Sb (Ref. 25) also creates a fertile ground for the occurrence of coupled magnetic and structural transformations. All these compounds consist of the same $^2_\infty[R_5T_4]$ slabs, strongly or weakly connected by T-T dimers, where T is Si, Ge, Ga, Sb, Sn, or their statistical mixtures.[26] The T-T bonds are not the only bonds that control the interslab interactions,[2,26,27] but they are the most characteristic ones determining basic physical and crystallographic properties. To date, there are five known basic structure types observed in the R_5T_4 systems: (i) the orthorhombic $Tm_5Si_2Sb_2$-type [space group (SG) is *Cmca*] where all interslab T-T dimers are broken and identical; (ii) the orthorhombic Sm_5Ge_4-type [often referred to as O(II)-type, SG *Pnma*] with all T-T dimers broken but no longer identical; (iii) the monoclinic $Gd_5Si_2Ge_2$-structure type (M-type, SG $P112_1/a$) with half of the T-T interslab dimers formed; (iv) the orthorhombic Gd_5Si_4-structure type [O(I)-type, SG *Pnma*]—all T-T dimers between the $^2_\infty[R_5T_4]$ slabs reformed,[6] and (v) low-temperature Ho_5Ge_4 structure ($M\beta$-type, SG $P12_1/m1$),[28] which is a monoclinically distorted variant of the Sm_5Ge_4 structure. It is worth noting that both Gd_5Si_4 and Sm_5Ge_4 structure types have the same symmetry of the lattice (SG *Pnma*) but they transform one into another via a martensite-like structural transition.[1,29]

The formation and breaking of the T-T dimers strongly affects exchange interactions between the ferromagnetically ordered $^2_\infty[R_5T_4]$ slabs and the resulting type of global magnetic ordering.[30] Therefore, by lowering temperature, changing chemical composition, applying magnetic field, or external pressure, modification of the T-T bonds can be achieved through a coupled magnetostructural transition, which in turn results in tuning the magnetic properties of R_5T_4 compounds.[6,26]

A detailed x-ray single crystal and powder diffraction study of $Gd_5Ga_xGe_{4-x}$ (Ref. 22) showed a sequence of structures similar to the $Gd_5(Si_xGe_{1-x})_4$ system when the concentration (x) of Ga varies. Mozharivskyj *et al.*[22] showed that substituting Ge with Ga, which lacks one electron in the outer shell (three valence electrons for Ga instead of four for Ge), drives a change in crystallography of the $Gd_5Ga_xGe_{4-x}$ system via a gradual reduction in the valence electron concentration, a mechanism similar to the one reported in $Gd_5Si_2Ge_2$.[2]

In a crystallographic study of several $R_5Sb_2(Si,Ge)_2$ alloys,[31] the $Tm_5Si_2Sb_2$-type structure was reported. It is closely related to the Sm_5Ge_4-type, but has a higher crystallographic symmetry (space group is *Cmca* instead of *Pnma*). $R_5Sb_2(Si,Ge)_2$ compounds with R=Y, Tb, Dy, Ho, Er, and Tm were reported, however, formation of the $Gd_5Sb_2Ge_2$ compound was not reported in Ref. 31. The formation of the $Gd_5Si_2Sb_2$ compound with the Sm_5Ge_4 crystal structure, which orders ferromagnetically at ~240 K, was later reported by Nirmala *et al.*[32]

Crystallographic, magnetic, electronic, and thermal measurements of polycrystalline samples of $Gd_5Sb_xGe_{4-x}$, where Ge was gradually substituted by Sb (antimony introduces an additional p electron), were recently reported.[25] The room temperature x-ray powder diffraction study[25] shows that the limit of Sb solubility in $Gd_5Sb_xGe_{4-x}$ is $x=2.7$. Higher concentrations of antimony lead into a multiple-phase region since the Gd_5Sb_4 composition does not exist. For $0 \leq x < 2$, the system adopts the Sm_5Ge_4-type of crystal structure. For $2 \leq x < 2.7$, the room temperature crystal structure is of the $Tm_5Si_2Sb_2$-type.

Magnetic measurements show that cooling triggers a first-order magnetic transition into the ferromagnetic (FM) state for low concentrations of Sb ($x<2$, Sm_5Ge_4-type) and a second-order transition to FM state for $2<x<2.7$ ($Tm_5Si_2Sb_2$-type). In the $Gd_5Sb_{0.5}Ge_{3.5}$ compound ($x=0.5$), the ferromagnetic ordering transition occurs at 37 K, and a second-order electronic transition at 60 K.[25] It was suggested that the antiferromagnetic (AFM) to paramagnetic (PM) transition also occurs at 60 K by analogy with the second-order transition observed at 130 K in Gd_5Ge_4.[16] This second-order transition does not occur when $x=1$ and 1.25, and there is only a first-order PM to FM transition on cooling. Additional anomalies in the dc magnetization and ac susceptibility were observed at ~150 and ~100 K for $x=0.5$ and $x=1$, respectively,[25] and these may be due to short-range magnetic clustering.

Among the $Gd_5Sb_xGe_{4-x}$ alloys, the $x=0.5$ composition appears to present the richest collection of physical phenomena, and a more detailed study of its structure-property relationships, especially the nature of its transitions is warranted. The low Sb content allows a comparison with the well-studied Gd_5Ge_4; it also can be compared with the recently reported properties of $Gd_5Si_{0.5}Ge_{3.5}$.[33] Here, we report investigation of the magnetic, thermal and crystallographic properties of the $Gd_5Sb_{0.5}Ge_{3.5}$ compound together with the electronic structure calculations intended to better understand some of the observed experimental findings.

II. EXPERIMENTAL AND THEORETICAL DETAILS

The single crystal of $Gd_5Sb_{0.5}Ge_{3.5}$ was grown in a tungsten crucible using the Bridgman technique.[34] The starting materials were Gd (99.86 at. % or 99.99 wt. % pure with respect to all elements) prepared by the Materials Preparation Center of the Ames Laboratory,[35] Sb (99.99 wt. %), and Ge (99.99 wt. %) both purchased from Meldform Metals (United Kingdom). The $Gd_5Sb_{0.5}Ge_{3.5}$ single crystal specimen for magnetic measurements was cut using a spark-eroding technique from a large grain as a parallelepiped with the approximate dimensions $1.00 \times 0.98 \times 1.55$ mm^3 with each side of the cube oriented perpendicular to one of the three principal crystallographic directions. Orientations were established using the back reflection Laue technique. The values of the demagnetization factors of the $Gd_5Sb_{0.5}Ge_{3.5}$ single crystal in magnetic field applied along the a, b, and c axes were 0.3, 0.25, and 0.23, respectively.[36] The sample for heat-capacity measurements was cut as a 6 mm in diameter by 2-mm-thick flat cylinder with the a axis aligned along the cylinder axis (and the magnetic field vector). The combined accuracy of the alignment of the crystallographic axes with the direction of the magnetic field vector was $\pm 5°$.

The sample for x-ray powder diffraction measurements was prepared by hand-grinding a small piece of the $Gd_5Sb_{0.5}Ge_{3.5}$ single crystal. The fine $Gd_5Sb_{0.5}Ge_{3.5}$ powder (particle size <25 μm) was mixed with a methanol diluted Ge varnish on a copper sample holder, air dried, and baked at 120 °C for 1 h in order to solidify the specimen and prevent rotation of individual particles in an applied magnetic field. The flat surface for the Bragg-Brentano diffraction experiment was created by using 320-grit sandpaper, thus minimizing preferred orientation near the surface and reducing surface roughness.[37]

The x-ray powder diffraction measurements were carried out as a function of temperature between 5 and 300 K in a zero magnetic field and between 5 and 100 K in constant magnetic fields ranging from 0 to 40 kOe on a Rigaku TTRAX rotating anode powder diffractometer employing Mo K_α radiation. The diffractometer was equipped with a continuous flow ^{4}He cryostat controlling the temperature of a sample with ± 0.05 K accuracy, and a split-coil superconducting magnet creating a homogeneous dc magnetic field around the specimen.[37] The Bragg peaks maximum intensity to lowest background intensity ratio was close to ~300 with the strongest Bragg peaks registering nearly 6000 counts at their peak values, which corresponds to ~1.8% statistical spread. The range of measured Bragg angles was from 9° to 49° 2θ, which is equivalent to ~19.5°–128° 2θ range using Cu Kα radiation ($\sin \theta_{max}/\lambda \approx 0.58$).

RIETICA LHPM software[38] was employed to carry out the full-profile Rietveld refinement of every recorded pattern. In the proximity of the transition, an attempt was made to refine both phases simultaneously. However, it was impossible to recognize both phases separately (the scale factor of one phase becomes negative) due to close positions of their Bragg reflections caused by the similar structures of the high-temperature and low-temperature phases. The isotropic thermal displacement parameters of all atoms in each phase were assumed to be the same, in effect, employing the overall isotropic thermal displacement approximation. The profile residuals R_p varied from ~0.09 to ~0.12, and the derived Bragg residuals R_B ranged from ~0.05 to ~0.09. The least-squares standard deviations of the refined lattice parameters were on the order of 20–30 ppm of the absolute values of the corresponding unit-cell dimensions.

The magnetic measurements were performed using an MPMS XL-7 SQUID magnetometer, manufactured by Quantum Design, Inc., which operates in the temperature interval 1.7–400 K and in magnetic fields up to 70 kOe. The accuracy of magnetic measurements was better than 1 %. The ac susceptibility was measured using the same magnetometer with the following parameters: $H_{dc}=0$, $H_{ac}=6$ Oe, and $f=125$ Hz. The heat capacity in magnetic fields up to 100 kOe was measured between ~2 and 350 K in a semiadiabatic heat pulse calorimeter, which has been described elsewhere.[39]

In order to have a better insight into the magnetism of $Gd_5Sb_{0.5}Ge_{3.5}$, first-principles electronic structure calculations have been performed. The local spin density approxi-

TABLE I. Crystal structure of $Gd_5Sb_{0.5}Ge_{3.5}$: high-temperature phase at 50 K, and low-temperature phase at 35 K; both have the Sm_5Ge_4 (O-II) structure. $T=75\%$ Ge+25% Sb.

Atom	x/a	y/b	z/c
HT-$Gd_5Sb_{0.5}Ge_{3.5}$, $T=50$ K, SG *Pnma*, $R_p=9.9\%$, $R_{wp}=12.8\%$ $a=7.7664(2)$ Å, $b=14.8552(4)$ Å, $c=7.8255(2)$ Å			
Gd1	0.2829(4)	0.2500	−0.0013(4)
Gd2	−0.0386(2)	0.1042(1)	0.1726(3)
Gd3	0.3860(2)	0.8822(1)	0.1652(3)
Ge1	0.1586(7)	0.2500	0.3662(9)
Ge2	0.9124(7)	0.2500	0.8807(8)
*T*3	0.2224(5)	0.9572(2)	0.4706(5)
LT-$Gd_5Sb_{0.5}Ge_{3.5}$, $T=35$ K, SG *Pnma*, $R_p=10.6\%$, $R_{wp}=13.6\%$, $a=7.7398(2)$ Å, $b=14.8690(4)$ Å, $c=7.8068(2)$ Å			
Gd1	0.2904(4)	0.2500	0.0007(3)
Gd2	−0.0319(2)	0.1015(1)	0.1768(3)
Gd3	0.3809(2)	0.8809(1)	0.1639(3)
Ge1	0.1700(7)	0.2500	0.3710(8)
Ge2	0.9200(7)	0.2500	0.8898(8)
*T*3	0.2194(5)	0.9578(2)	0.4671(5)

mation including Hubbard U parameter (LSDA+U) approach[40,41] has been employed within the scalar relativistic version of the tight binding linear muffin tin orbital (TB-LMTO) (Ref. 42) method. We used $U=6.7$ eV and $J=0.7$ eV—the well-known values for Gd atoms. The conventional von Barth and Hedin parameterization of the LSDA (Ref. 43) has been adopted. Furthermore, 125 special k points have been used in the irreducible part of the Brillouin zone for k space integration in the orthorhombic Sm_5Ge_4 (O-II) structure of $Gd_5Sb_{0.5}Ge_{3.5}$.

III. EXPERIMENTAL RESULTS

According to the temperature dependent x-ray powder diffraction, the $Gd_5Sb_{0.5}Ge_{3.5}$ compound, which has the Sm_5Ge_4-type of crystal structure (Table I) undergoes a structural (volume change) transition at 40 K without a major rearrangement of its crystallographic structure. This is the temperature at which the Bragg peaks of the low-temperature phase begin to emerge. The two phases coexist over a relatively narrow (5 K) range of temperatures.

Figure 1 presents the temperature dependencies of lattice parameters and unit-cell volume of $Gd_5Sb_{0.5}Ge_{3.5}$, measured during heating and cooling of the sample in 0 kOe and during heating of the sample in 20 and 40 kOe magnetic fields. Steps in the lattice parameters correspond to the transition that shifts to higher temperatures in applied magnetic fields. The largest relative change in the lattice parameter is observed along the a direction ($\Delta a/a=-0.32\%$), whereas changes along the c and b directions are $\Delta c/c=-0.23\%$ and $\Delta b/b=0.08\%$, respectively (Fig. 1). Similar discontinuities were observed when the structural transition was induced by the application of the magnetic field (Fig. 2). It is worth

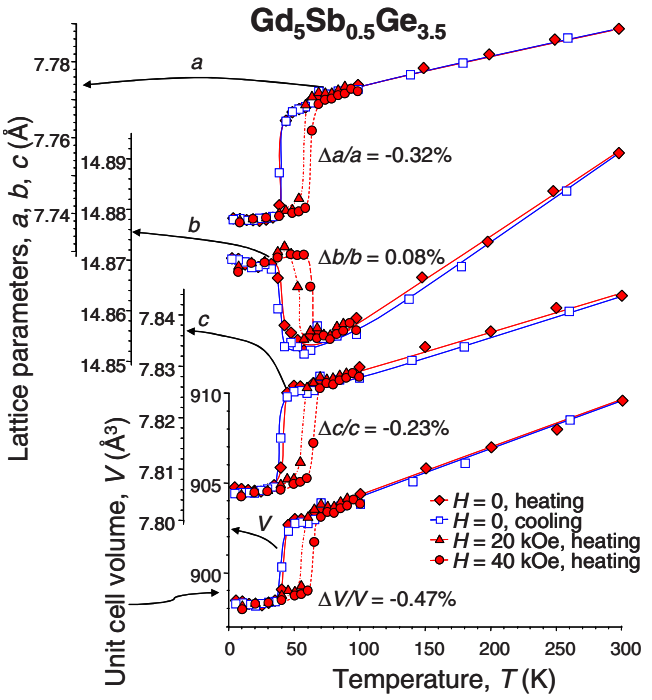

FIG. 1. (Color online) Temperature dependencies of the lattice parameters and the unit-cell volume of $Gd_5Sb_{0.5}Ge_{3.5}$ in the temperature interval from 5 to 300 K in a zero magnetic field on heating and cooling, and in 20 and 40 kOe magnetic fields on heating.

noting that the changes along the a and c axes are of the same sign, unlike those in Gd_5Ge_4 and $Gd_5Si_{0.5}Ge_{3.5}$, where the major change occurs along the a axis (−1.8%) and the change along the c axis is of the opposite sign and is three times smaller.[33,37] The thermal expansion is largest along the b axis, which undergoes smaller change at the transition—this effect is commonly observed in other R_5T_4 systems.[33]

Due to nearly identical crystal structures (and, therefore, almost identical diffraction patterns) of the low-temperature (LT) and high-temperature (HT) phases, it was impossible to reliably determine structural parameters of the individual phases in the region of phase coexistence. Thus, the points in the vicinity of the transition (i.e., at 40 K for zero field data) represent the average lattice parameters of the two phases. Temperature hysteresis is fairly small (5 K) and is similar to $Gd_5Si_{0.5}Ge_{3.5}$. The shift in the transition temperature with the magnetic field is nonlinear: for a magnetic field change from 0 to 20 kOe the transition temperature shifts by ~15 K, which is greater than that from 20 to 40 kOe (~10 K), this is quite evident in Fig. 1.

Figure 1 also shows the change in the unit-cell volume of $Gd_5Sb_{0.5}Ge_{3.5}$ with temperature, and Fig. 2 shows the change in the unit-cell volume during isothermal magnetization and demagnetization at 55 K. Even though the $\Delta V/V=-0.47\%$ is quite large in $Gd_5Sb_{0.5}Ge_{3.5}$, and it agrees with the first-order nature of the transition, this is only 40% of that observed in $Gd_5Si_{0.5}Ge_{3.5}$ (−1.16%).[33] However, the mechanism of the transition is substantially different from the earlier reported crystallographic transitions found in other $R_5(Si_xGe_{1-x})_4$ systems. In our case, there are no large shear displacements of the slabs with respect to one another (Table II), and no

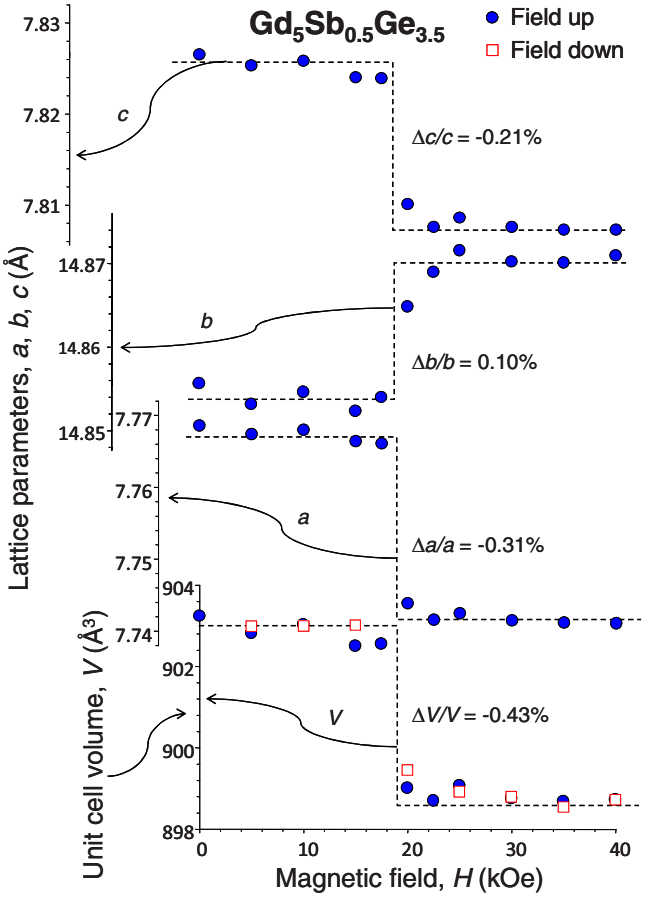

FIG. 2. (Color online) The isothermal behavior of the lattice parameters and the unit-cell volume of the $Gd_5Sb_{0.5}Ge_{3.5}$ at 55 K measured on applying a magnetic field from 0 to 40 kOe and then lowering the field back to zero (the demagnetization is shown for the unit-cell volume only).

change in the lattice symmetry as well. On the other hand, some atomic rearrangement is indeed present as a result of the adaptation to a new magnetic state, and this will be discussed below.

The heat capacity of $Gd_5Sb_{0.5}Ge_{3.5}$ single crystal from 2 to 200 K in magnetic fields ranging from 0 to 100 kOe, applied along the *a* axis is presented in Fig. 3. The sharp peak characteristic of first-order transition moves to higher

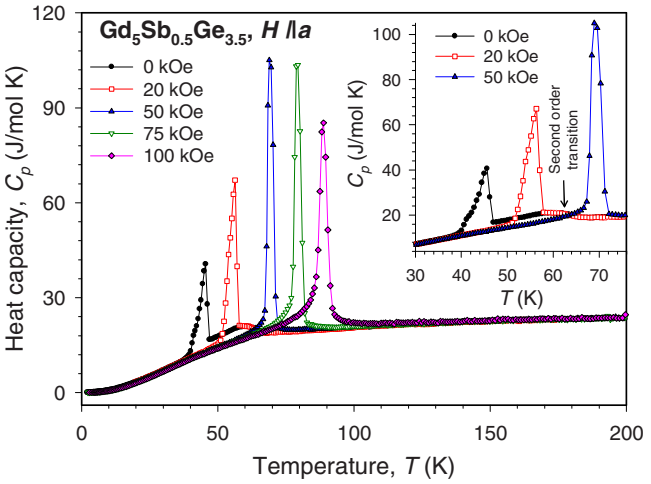

FIG. 3. (Color online) The temperature dependence of the heat capacity of $Gd_5Sb_{0.5}Ge_{3.5}$ single crystal over the temperature interval of 2–200 K in magnetic fields up to 100 kOe applied along the *a* axis. The inset highlights the second-order transition observed at ~63 K.

temperatures with the application of magnetic field and the peak retains its first-order shape even in 100 kOe field. A weak second-order transition is present at 63 K in 0 and 20 kOe magnetic fields and is more obvious in the inset of Fig. 3. This second-order anomaly is essentially field independent and appears the same for 0 and 20 kOe field data. However, when the temperature of the first-order transition exceeds 63 K (in magnetic fields of 50 kOe and above) the second-order anomaly disappears indicating that it is specific to the high-temperature phase. These results are in a full agreement with previous measurements carried out on a polycrystalline material.[25]

The isothermal magnetization of $Gd_5Sb_{0.5}Ge_{3.5}$ at temperatures from 2 to 200 K with the magnetic field applied along the *a* crystallographic direction is presented in Fig. 4. The sharp metamagnetic steps of the magnetization shifting to higher magnetic fields when temperature increases are observed between 40 and 75 K indicating field-induced magnetostructural transition into the FM state. Note, that the isothermal x-ray powder diffraction data collected at 55 K (Fig. 2) also show a transition around 20 kOe, and are in good agreement with $M(H)$ and heat-capacity data. The narrow

TABLE II. The interatomic distances most affected by structural transition (changed more than 1%). T =75% Ge+25% Sb.

	HT-$Gd_5Sb_{0.5}Ge_{3.5}$, T=50 K	LT-$Gd_5Sb_{0.5}Ge_{3.5}$, T=35 K	
Atomic pairs	Distances, d (Å)	Distances, d (Å)	Change, $d_{50\ K}-d_{35\ K}$, %
Ge1-Ge2	2.795(9)	2.689(9)	−3.94
Gd2-*T*3	3.784(4)	3.672(4)	−3.04
Gd3-Ge1	3.075(6)	3.029(5)	−1.51
*T*3-*T*3	3.710(7)	3.658(7)	−1.42
Gd2-Ge1	3.054(5)	3.101(5)	1.52
Gd1-Ge2	3.135(7)	3.209(6)	2.31

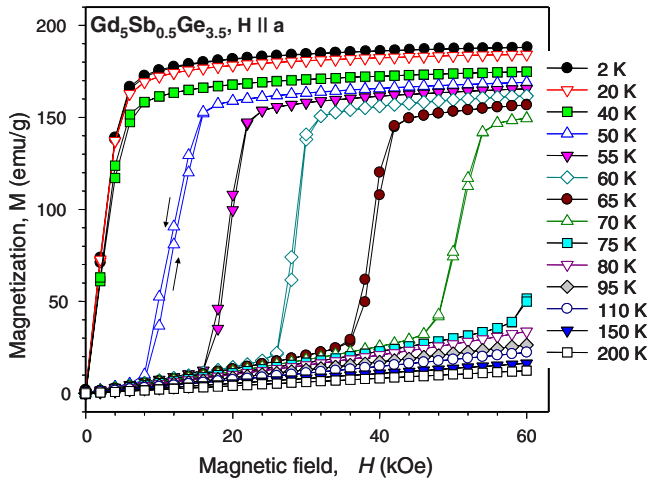

FIG. 4. (Color online) The isothermal magnetization of $Gd_5Sb_{0.5}Ge_{3.5}$ single crystal over the temperature interval from 2 to 200 K in magnetic fields up to 60 kOe, applied along the *a* axis. The arrows shown near the 50 K isotherm indicate the direction of the magnetic field change.

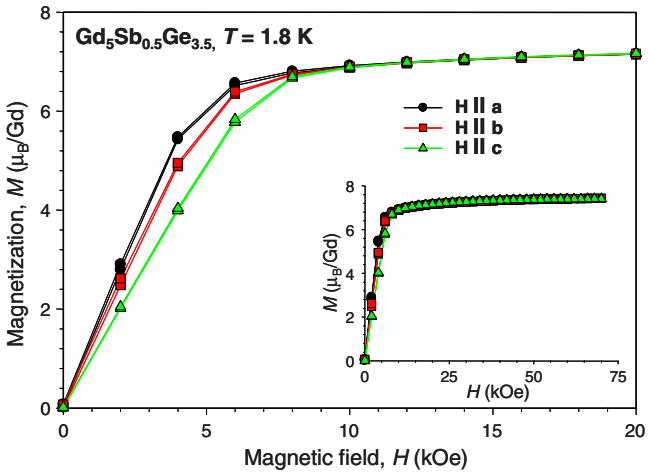

FIG. 5. (Color online) The isothermal magnetization of $Gd_5Sb_{0.5}Ge_{3.5}$ single crystal at 1.8 K measured as a function of magnetic field applied along *a*, *b*, and *c* axes. The main panel displays low field details, and the inset shows the $M(H)$ data in fields up to 70 kOe.

magnetic field hysteresis (<1 kOe), comparable to that observed in the $Gd_5Si_{0.5}Ge_{3.5}$,[33] is worth noting. The isothermal magnetization with magnetic fields applied along the *b* and *c* axes is similar, and, therefore, not shown here.

To determine the easy magnetization direction the magnetization isotherms were measured along *a*, *b*, and *c* axes at 1.8 K, well below the ordering temperature (Fig. 5). Unlike Gd_5Ge_4, where the easy magnetization axis is the *b* direction, the easy axis in $Gd_5Sb_{0.5}Ge_{3.5}$ is the *a* direction. The *c* direction is the hard magnetization axis in both Gd_5Ge_4 and $Gd_5Sb_{0.5}Ge_{3.5}$. However, the difference between the three crystallographic directions is smaller in $Gd_5Sb_{0.5}Ge_{3.5}$ than in Gd_5Ge_4 meaning that the magnetic anisotropy is weaker in $Gd_5Sb_{0.5}Ge_{3.5}$. The value of the saturation magnetization is 187.1 emu/g or $7.38\mu_B$ per Gd atom, which is in good agreement with the $7.38\mu_B$/Gd value calculated from first principles when placing the Sb atoms in the *T*3 and Ge in the *T*1 and *T*2 sites (see Table III).

The temperature dependencies of the real and imaginary parts of the *ac* susceptibility of $Gd_5Sb_{0.5}Ge_{3.5}$ with ac field applied along the *a*, *b*, and *c* axes are presented in Figs. 6 and 7, respectively. The main paramagnetic-to-ferromagnetic transition occurs around 40 K in all data sets. Several weaker anomalies, such as a peak around 140 K in case of $\mathbf{H}\|\mathbf{a}$ and $\mathbf{H}\|\mathbf{c}$, and a steplike anomaly around 160 K with $\mathbf{H}\|\mathbf{b}$ and $\mathbf{H}\|\mathbf{c}$ are observed. The nonzero imaginary part of the susceptibility, especially with $\mathbf{H}\|\mathbf{c}$ in the temperature interval 60–180 K is related to magnetic losses in the sample at temperatures much higher than the long-range magnetic ordering temperature indicating possible strong short-range order interactions. The latter are due to competing interslab and intraslab exchange interactions and/or to the Griffiths phaselike behavior observed in many other members of the R_5T_4 family.[27,44–46] No magnetic transition is detected at ~63 K indicating that the second-order transition observed from heat-capacity data in 0 and 20 kOe magnetic fields does not have a magnetic origin and therefore cannot be a paramagnetic-to-antiferromagnetic transition as was suggested before.[25]

IV. DISCUSSION OF THE EXPERIMENTAL RESULTS

The presence of the sharp first-order magnetostructural transition in $Gd_5Sb_{0.5}Ge_{3.5}$ is similar to the behavior of the $Gd_5(Si_xGe_{1-x})_4$ alloys, for example, $Gd_5Si_{0.5}Ge_{3.5}$.[33] However, the temperature and field dependent x-ray powder diffraction data show that unlike Gd_5Ge_4 and $Gd_5Si_{0.5}Ge_{3.5}$, where the first-order transition occurs with the martensitic-like change in the crystal structure from the Sm_5Ge_4 type to the Gd_5Si_4 type, in $Gd_5Sb_{0.5}Ge_{3.5}$ the first-order transition does not involve shear displacements of the $^2_\infty[Gd_5T_4]$ slabs (Table II).

In Gd_5Ge_4 (as well as in $Gd_5Si_{0.5}Ge_{3.5}$), the largest change in lattice dimensions during the structural transition occurs along the *a* axis and the relative change $(\Delta a/a)$ is equal to −1.8%,[29,33] which is more than five times greater than $\Delta a/a=-0.32\%$, observed in $Gd_5Sb_{0.5}Ge_{3.5}$ (see Fig. 1). This large change in the *a*-lattice parameter in Gd_5Ge_4 is related to the shear displacements of adjacent $^2_\infty[Gd_5T_4]$ slabs and results in a drastic ~30% shortening of the interslab *T*3-*T*3 distances, resulting in the formation of strong *T*3-*T*3 bonds. The negative change (−1.8%) in the Gd_5Ge_4 of the *a*-lattice

TABLE III. Atom projected magnetic moments (in μ_B/atom) with Ge3 (Sb3) in *T*3 positions.

Gd1-4*c*	Gd2-8*d*	Gd3-8*d*	Gd, average	Ge1-4*c*	Ge2-4*c*	Ge3-8*d*
7.36(7.56)	7.23(7.38)	7.21(7.29)	7.25(7.38)	0.02(0.02)	0.03(0.02)	−.02(0.02)

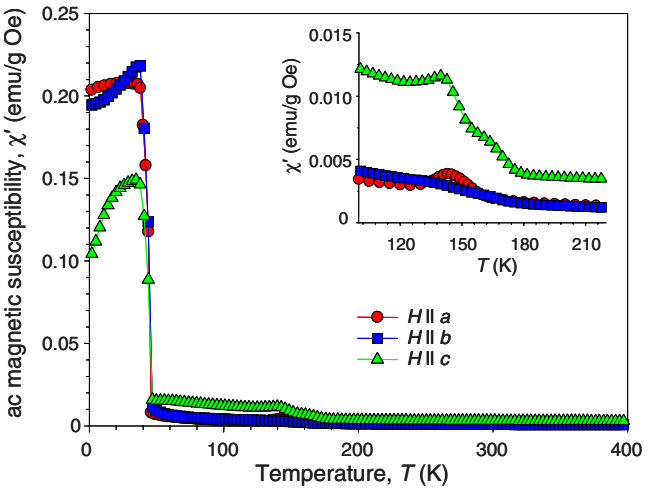

FIG. 6. (Color online) The temperature dependence of the real component of ac magnetic susceptibility of $Gd_5Sb_{0.5}Ge_{3.5}$ single crystal over the temperature interval 2–250 K (*a* axis) and 2–400 K (*b* and *c* axes) in a zero dc magnetic field. The data were collected at a frequency of 125 Hz and ac field of 6 Oe. The inset shows the region between 100 and 220 K.

parameter is accompanied by smaller increases in *b*- and *c*-lattice parameters by ~0.14% and ~0.6%,[29] respectively. The giant volume change of Gd_5Ge_4 (−1%) mostly comes from the decrease in the *a*-lattice parameter.

In $Gd_5Sb_{0.5}Ge_{3.5}$, the changes are of the same sign (Figs. 1 and 2) along the *a* and *c* axes: $\Delta a/a=-0.32\%$ and $\Delta c/c=-0.23\%$, respectively. The $^2_\infty[Gd_5T_4]$ slabs in $Gd_5Sb_{0.5}Ge_{3.5}$ do not shift with respect to each other, but they simply contract in the *ac* plane. As illustrated in Table II, the most affected interatomic distances are the intraslab Ge1-Ge2 distances, where one can see approximately −4% shortening, and the intraslab Gd-Ge distances, which experience an average ~2% increase. The contraction of the $^2_\infty[Gd_5T_4]$ slabs in the *ac* plane affects the *b*-lattice parameter, which slightly increases by 0.08 % (see Fig. 1). Unlike Gd_5Ge_4, it is not the interslab Ge–Ge bond distances that change significantly during the transition in $Gd_5Sb_{0.5}Ge_{3.5}$, but the intraslab Ge-Ge distances, which decrease by 4 % (see Table II). This is an interesting fact because it is well established that making and breaking of the interslab *T*-*T* bonds in $Gd_5(Si,Ge)_4$ couples magnetic and structural transition by switching on and off the exchange interaction between Gd atoms located inside neighboring slabs.[2,26] Apparently, it is not the case of $Gd_5Sb_{0.5}Ge_{3.5}$, as will be shown below by first-principles electronic structure calculations. In $Gd_5Sb_{0.5}Ge_{3.5}$ the Sm_5Ge_4-type becomes compatible with the FM ground state.

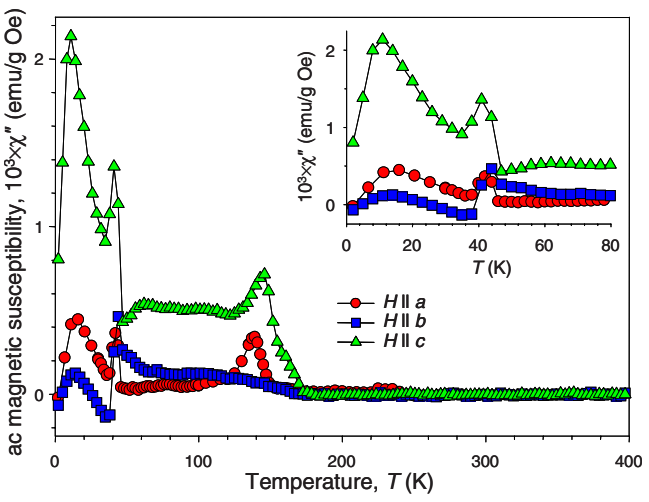

FIG. 7. (Color online) The temperature dependence of the imaginary component of ac magnetic susceptibility of $Gd_5Sb_{0.5}Ge_{3.5}$ single crystal over the temperature interval 2–250 K (*a* axis) and 2–400 K (*b* and *c* axes) in a zero dc magnetic field. The data were collected at a frequency of 125 Hz and ac field of 6 Oe. The inset shows the region between 2 and 80 K.

The second-order transition observed at 60 K in $Gd_5Sb_{0.5}Ge_{3.5}$ from heat-capacity and electrical resistivity[25] shows some similarity to the transition at 130 K in pure Gd_5Ge_4. In both compounds, the heat capacity exhibits a second-order transition and electrical resistivity shows a peak at 60 and 130 K in $Gd_5Sb_{0.5}Ge_{3.5}$ and Gd_5Ge_4, respectively. However, in Gd_5Ge_4 the transition is clearly seen in the magnetic data while in $Gd_5Sb_{0.5}Ge_{3.5}$ there is no indication of a magnetic ordering at the second-order transition temperature.

V. ELECTRONIC STRUCTURE CALCULATIONS

In order to gain insight into the experimental results of $Gd_5Sb_{0.5}Ge_{3.5}$ described above, we have performed first-principles electronic structure calculations. Experimental observations show that the ground state crystal structure of $Gd_5Sb_{0.5}Ge_{3.5}$ is Sm_5Ge_4-type orthorhombic [O(II)] structure and the Sb atoms prefer the interslab *T*3 positions of the O(II) Gd_5Ge_4 (see Table I). In order to see whether this preferential occupation agrees with theory, the formation energies, $\Delta E_f=E_{Gd_5Sb_{0.5}Ge_{3.5}}-c_{Gd}E_{Gd}-c_{Ge}E_{Ge}-c_{Sb}E_{Sb}$, where, *E* and *c* represent total energies and concentrations, respectively, have been calculated while placing Sb atoms in the individual positions of the Ge atoms in the O(II) polymorph of Gd_5Ge_4. Calculations indeed show that the lowest formation energy is when Sb replaces Ge3 (interslab) in the O(II) Gd_5Ge_4 and confirm the experimental observation pointed above. It is interesting to note that while substituting Si for Ge in the O(II) Gd_5Ge_4, the lowest energy is when the Ge1,2 (intraslab) sites are replaced by Si. This may indicate that atoms with extra *p* electrons occupy interslab positions and the isoelectronic atoms occupy intraslab positions in the O(II) structure of Gd_5Ge_4.[24,33]

Figure 8 shows formation energy as a function of the unit-cell volume considering either Ge atoms or Sb atoms in the *T*3 positions. Here, the equilibrium unit-cell volume corresponding to total energy minima is found by the variation in the lattice constant *a*. Calculations also show the same equilibrium volumes with the variation in other lattice constants *b* and/or *c*. The equilibrium unit-cell volume changes from 856.5 to 861.2 $Å^3$ when Ge is replaced by Sb in the *T*3 sites. It is important to note that there is substantial lowering of the formation energy with Sb substitution (Fig. 8) indicating that this substitution is energetically favorable.

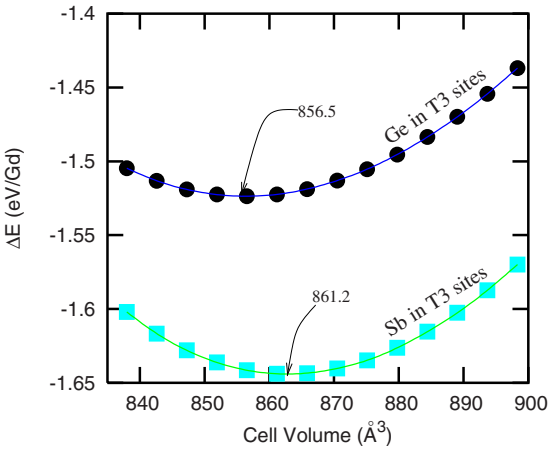

FIG. 8. (Color online) Variation of energy of formation as a function of unit-cell volume with Ge or Sb atoms in the $T3$ positions of $Gd_5Sb_{0.5}Ge_{3.5}$.

The $4f$ moments ($7\mu_B$/Gd) in $Gd_5Sb_{0.5}Ge_{3.5}$ spin polarize the conduction ($5d$) electrons through the indirect Ruderman-Kittel-Kasuya-Yosida (RKKY) interactions. These interactions cause exchange splitting in the majority and minority spin bands and give rise to $5d$ magnetic moments. The nonequivalent Gd atoms have different $5d$ moments depending on the nearest neighbor coordination. Interestingly, we find that both the exchange splitting and polarization in the $5d$ density of states at the Fermi level increase by 15 % when the Ge3 site is substituted by the Sb atom. This confirms that the Sb atom enhances ferromagnetism when it replaces Ge atoms in Gd_5Ge_4. Table III shows the atom projected magnetic moments in $Gd_5Sb_{0.5}Ge_{3.5}$. On the average, there is a 52 % increase in $5d$ moments (from 0.25 to 0.38μ_B) when Sb replaces interslab Ge atoms. The p states of Sb lift up the antibonding states of Ge appearing around the Fermi level. This forms a stronger ferromagnetic bridge between the nearest neighbor slabs in $Gd_5Sb_{0.5}Ge_{3.5}$, and this is the reason that the interatomic distances between the neighboring slabs change less than 2% during the ferromagnetic transition.

Furthermore, the stability of the O(II) structure in $Gd_5Sb_{0.5}Ge_{3.5}$ may arise due the higher number of p electrons in Sb compared to Ge as pointed above. Since, the p-d hybridization influences the indirect $4f$-$4f$ exchange (RKKY) in Gd_5Ge_4,[30,47] the enhanced p states should have a critical role in ferromagnetism of the O(II) structure of $Gd_5Sb_{0.5}Ge_{3.5}$, otherwise it should have an antiferromagnetic state as the ground state as is the case for O(II) Gd_5Ge_4. It is interesting to note that when one alternatively substitutes Sn instead of Sb in the $T3$ site the O(II) structure remains in the AFM state, and O(I) is the ferromagnetic structure. Like antimony, the tin atoms are larger than Ge atoms, but Sn does not have an extra p electron and it is isoelectronic to Ge so the p-d hybridization here does not support ferromagnetism in the O(II) structure. The strong influence of an extra p electron on the crystal structure of the Gd_5T_4 compounds was recently observed in $Gd_5Si_{4-x}P_x$ series as well.[48] In the case of $Gd_5Si_{0.5}Ge_{3.5}$, although Si is isoelectronic to Ge, the chemical pressure plays a determining role of creating ferromagnetism in $Gd_5(Si_xGe_{1-x})_4$ compounds.[33,49]

The densities of states (DOS) of nonequivalent Gd atoms in $Gd_5Sb_{0.5}Ge_{3.5}$ differ from one another. The spin up DOS at the Fermi level (E_F) of Gd1 atom, located at the center of the slabs is higher than the spin up DOS (E_F) of other Gd atoms (Gd2 and Gd3), located on the edges of the slabs (see Table III). On the other hand, the spin down DOS (E_F) of nonequivalent Gd atoms are identical. This shows that the Gd1 has higher spin polarization and magnetic moment compared to the other two nonequivalent Gd atoms.

Figure 9 shows density of states around the Fermi level of Gd1, Ge, and Sb atoms in $Gd_5Sb_{0.5}Ge_3$. The spin down DOS of Ge in the $T3$ site at and just below the Fermi level is higher compared to the spin up counterpart. These spin down $4p$ states of Ge atom in the $T3$ site strongly overlap with the spin down $5d$ states of Gd atoms and act like the spin down $5d$ states, which results in confining large number of conduction electrons in the spin down direction. Because of this confinement, there is less spin polarization of the $5d$ electrons of Gd when $T3$ site is occupied by Ge. On the other hand, when Sb occupies the $T3$ site, there are almost identical spin up and spin down $5p$ electrons of Sb at the Fermi level and they hybridize equally with the $5d$ states of Gd in both spin directions. In this case, there is no conduction electron confinement in the spin down direction and therefore there is higher spin polarization of the $5d$ states of Gd at the Fermi level with Sb atoms in the $T3$ sites.

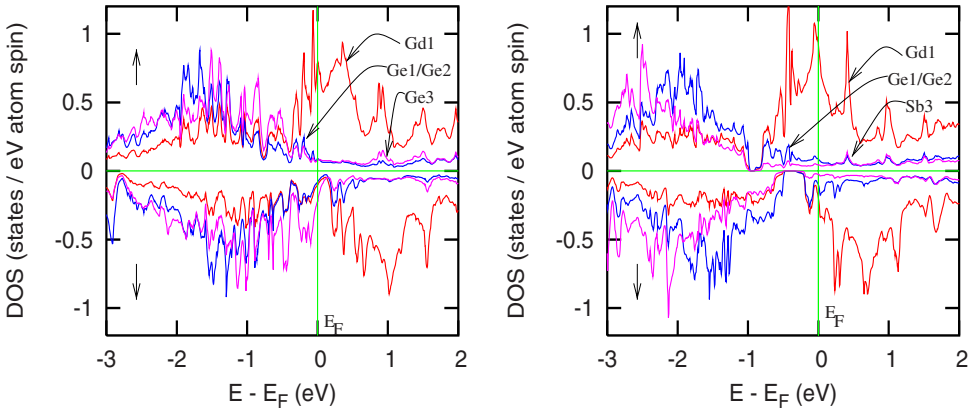

FIG. 9. (Color online) Density of states (DOS) of Gd1 atoms, which connects the inter- and intraslab-Gd-Ge/Sb-Ge/Sb-Gd- and -Gd-Ge-Ge-Gd-networks and that of Ge (left diagram) and Sb (right diagram) atoms in $Gd_5Sb_{0.5}Ge_{3.5}$.

TABLE IV. Intraslab and interslab magnetic exchange interactions (in meV) with Ge or Sb in $T3$ sites of $Gd_5Sb_{0.5}Ge_{3.5}$ (low-temperature structure, 15 K).

	Intraslab	Interslab
Ge in $T3$ position	13.4	19.3
Sb in $T3$ position	26.1	30.5

Several experimental studies[50,51] show that the neighboring slabs, which are themselves ferromagnetic, are aligned ferromagnetically in O(I)-Gd_5Ge_4 but they are antiferromagnetically aligned in the O(II)-Gd_5Ge_4 polymorph. Interestingly, $Gd_5Sb_{0.5}Ge_{3.5}$ does not show the same structural transformation and the O(II) polymorph itself is ferromagnetic at low temperature. In order to understand this phenomena, we model the magnetic exchange interactions using the Heisenberg approach by considering interactions between the Gd spins of nearest neighbor slabs (interslab interactions) as well as the Gd spins within the individual slabs (intraslab interactions). The interslab interactions are estimated by calculating the total energy difference between the artificially imposed AFM and FM aligned nearest neighbor slabs as described below. In these calculations, the O(II) structure with *Pnma* symmetry has been converted into the equivalent triclinic structure with $P1$ symmetry so that each of the 36 atoms in the unit cell are formally nonequivalent to any other atom in the same unit cell.[27] This helps to assign the specific configuration of Gd spins. Here, the AFM structure is constructed in such a way that 10 Gd atoms/cell that belong to the same slab are aligned ferromagnetically but the remaining 10 Gd atoms/cell that belong to the neighboring slab are aligned ferromagnetically in the opposite direction. The AFM configuration for intraslab interactions is modeled by making five Gd spins in each slab up and five down). This approach to calculation of inter- and intraslab exchange interactions takes into account both localized and conduction electrons contributions to the exchange interactions unlike the exchange interactions between correlated $4f$ states only.[40]

Table IV shows intra- and interslab magnetic exchange interactions with Ge or Sb in $T3$ positions in $Gd_5Sb_{0.5}Ge_{3.5}$. The interslab exchange interactions are higher than that of the intraslab exchange interactions contrary to that in the AFM O(II) Gd_5Ge_4.[27] Even in the FM O(I) Gd_5Ge_4, the intra- and interslab exchange interactions are identical. The enhancement of the interslab magnetic exchange interactions in $Gd_5Sb_{0.5}Ge_{3.5}$ due to the presence of Sb is likely the main reason why no antiferromagnetic order has been observed experimentally in $Gd_5Sb_{0.5}Ge_{3.5}$.

VI. CONCLUSIONS

The coupled magnetostructural transition in $Gd_5Sb_{0.5}Ge_{3.5}$ in the temperature interval from 40 to 85 K and in magnetic fields from 0 to 100 kOe is characterized by a large volume change ($\Delta V/V \cong -0.5\%$) without the displacement of the $^2_\infty[Gd_5T_4]$ slabs. The first-order transition in $Gd_5Sb_{0.5}Ge_{3.5}$ occurs without a change in the crystal structure type—the Sm_5Ge_4-type is preserved in both the LT and HT phases. The main changes during the transition consist of the atomic rearrangement within the slabs.

The first-order transition in $Gd_5Sb_{0.5}Ge_{3.5}$ is a ferromagnetic to paramagnetic ordering transition while the second-order transition at 63 K observed in the heat-capacity data does not have a magnetic origin.

The Sb substitution into the interslab positions of the Sm_5Ge_4-type structure increases the ferromagnetic exchange interactions between the slabs in $Gd_5Sb_{0.5}Ge_{3.5}$ compound to the point when the slab shifts and formation of the $T3$-$T3$ bonds are no longer needed to promote the ferromagnetic ground state.

ACKNOWLEDGMENTS

The Ames Laboratory is operated by Iowa State University of Science and Technology for the U.S. Department of Energy under Contract No. DE-AC02-07CH11358. Work at Ames Laboratory is supported by the Office of Basic Energy Sciences, Materials Sciences Division of the Office of Science.

*Present address: Physics Department, Purdue University, West Lafayette, Indiana, 47907-2036, USA.

†Corresponding author; vitkp@ameslab.gov

[1] L. Morellon, P. A. Algarabel, M. R. Ibarra, J. Blasco, B. Garcia-Landa, Z. Arnold, and F. Albertini, Phys. Rev. B **58**, R14721 (1998).

[2] W. Choe, V. K. Pecharsky, A. O. Pecharsky, K. A. Gschneidner, Jr., V. G. Young, Jr., and G. J. Miller, Phys. Rev. Lett. **84**, 4617 (2000).

[3] D. A. Filippov, R. Z. Levitin, A. N. Vasil'ev, T. N. Voloshok, H. Kageyama, and R. Suryanarayanan, Phys. Rev. B **65**, 100404(R) (2002).

[4] C. P. Sasso, M. Pasquale, L. Giudici, S. Besseghini, E. Villa, L. H. Lewis, T. A. Lograsso, and D. L. Schlagel, J. Appl. Phys. **99**, 08K905 (2006).

[5] V. K. Pecharsky and K. A. Gschneidner, Jr., in *Magnetism and Structure in Functional Materials*, edited by A. Planes, L. Manosa, and A. Saxena, Springer Series in Materials Science Vol. 79 (Springer-Verlag, Heidelberg, 2005), Chap. 11, p. 199.

[6] V. K. Pecharsky and K. A. Gschneidner, Jr., Pure Appl. Chem. **79**, 1383 (2007) and references therein.

[7] V. K. Pecharsky and K. A. Gschneidner, Jr., Phys. Rev. Lett. **78**, 4494 (1997).

[8] Ya. Mudryk, Y. Lee, T. Vogt, K. A. Gschneidner, Jr., and V. K. Pecharsky, Phys. Rev. B **71**, 174104 (2005).

[9] G. J. Miller, Chem. Soc. Rev. **35**, 799 (2006).

[10] C. Magen, Z. Arnold, L. Morellon, Y. Skorokhod, P. A. Algarabel, M. R. Ibarra, and J. Kamarad, Phys. Rev. Lett. **91**, 207202

(2003).
[11] V. K. Pecharsky and K. A. Gschneidner, Jr., Appl. Phys. Lett. **70**, 3299 (1997).
[12] V. K. Pecharsky and K. A. Gschneidner, Jr., Adv. Cryog. Eng. **43**, 1729 (1998).
[13] L. Morellon, J. Stankiewicz, B. Garcia-Landa, P. A. Algarabel, and M. R. Ibarra, Appl. Phys. Lett. **73**, 3462 (1998).
[14] E. M. Levin, A. O. Pecharsky, V. K. Pecharsky, and K. A. Gschneidner, Jr., Phys. Rev. B **63**, 064426 (2001).
[15] L. Morellon, P. A. Algarabel, C. Magen, and M. R. Ibarra, J. Magn. Magn. Mater. **237**, 119 (2001).
[16] E. M. Levin, V. K. Pecharsky, and K. A. Gschneidner, Jr., Phys. Rev. B **63**, 174110 (2001).
[17] F. Casanova, A. Labarta, X. Batlle, E. Vives, J. Marcos, L. Mañosa, and A. Planes, Eur. Phys. J. B **40**, 427 (2004).
[18] S. B. Roy, M. K. Chattopadhyay, P. Chaddah, J. D. Moore, G. K. Perkins, L. F. Cohen, K. A. Gschneidner, Jr., and V. K. Pecharsky, Phys. Rev. B **74**, 012403 (2006).
[19] V. Hardy, S. Majumdar, S. Crowe, M. R. Lees, D. M. Paul, L. Hervé, A. Maignan, S. Hébert, C. Martin, C. Yaicle, M. Hervieu, and B. Raveau, Phys. Rev. B **69**, 020407(R) (2004).
[20] J. Leib, J. E. Snyder, T. A. Lograsso, D. Schlagel, and D. C. Jiles, J. Appl. Phys. **95**, 6915 (2004).
[21] J. D. Moore, G. K. Perkins, Y. Bugoslavsky, L. F. Cohen, M. K. Chattopadhyay, S. B. Roy, P. Chaddah, K. A. Gschneidner, Jr., and V. K. Pecharsky, Phys. Rev. B **73**, 144426 (2006).
[22] Yu. Mozharivskyj, W. Choe, A. O. Pecharsky, and G. J. Miller, J. Am. Chem. Soc. **125**, 15183 (2003).
[23] D. H. Ryan, M. Elouneg-Jamróz, J. van Lierop, Z. Altounian, and H. B. Wang, Phys. Rev. Lett. **90**, 117202 (2003).
[24] Y. Mozharivskyj, A. O. Tsokol, and G. J. Miller, Z. Kristallogr. **221**, 493 (2006).
[25] A. S. Chernyshov, Ya. S. Mudryk, V. K. Pecharsky, and K. A. Gschneidner, Jr., J. Appl. Phys. **99**, 08Q102 (2006).
[26] V. K. Pecharsky and K. A. Gschneidner, Jr., Adv. Mater. **13**, 683 (2001).
[27] D. Paudyal, V. K. Pecharsky, and K. A. Gschneidner, Jr., J. Phys.: Condens. Matter **20**, 235235 (2008).
[28] N. K. Singh, Durga Paudyal, Ya. Mudryk, V. K. Pecharsky, and K. A. Gschneidner, Jr., Phys. Rev. B **79**, 094115 (2009).
[29] V. K. Pecharsky, A. P. Holm, K. A. Gschneidner, Jr., and R. Rink, Phys. Rev. Lett. **91**, 197204 (2003).
[30] D. Haskel, Y. B. Lee, B. N. Harmon, Z. Islam, J. C. Lang, G. Srajer, Ya. Mudryk, K. A. Gschneidner, Jr., and V. K. Pecharsky, Phys. Rev. Lett. **98**, 247205 (2007).
[31] A. Yu. Kozlov, V. V. Pavlyuk, and V. M. Davydov, Intermetallics **12**, 151 (2004).
[32] R. Nirmala, A. V. Morozkin, and S. K. Malik, EPL **72**, 652 (2005).
[33] Ya. Mudryk, D. Paudyal, V. K. Pecharsky, and K. A. Gschneidner, Jr., Phys. Rev. B **77**, 024408 (2008).
[34] D. L. Schlagel, T. A. Lograsso, A. O. Pecharsky, and J. A. Sampaio, in *Light Metals 2005*, edited by H. Kvande (The Minerals, Metals and Materials Society, Warrendale, PA, 2005), p. 1177.
[35] Materials Preparation Center, The Ames Laboratory U.S. Department of Energy, Ames, IA, USA, www.mpc.ameslab.gov
[36] A. Aharoni, J. Appl. Phys. **83**, 3432 (1998).
[37] A. P. Holm, V. K. Pecharsky, K. A. Gschneidner, Jr., R. Rink, and M. N. Jirmanus, Rev. Sci. Instrum. **75**, 1081 (2004).
[38] B. Hunter, Rietica: A Visual Rietveld Program, International Union of Crystallography Commission on Powder Diffraction Newsletter No. 20, Summer, 1998 (http://www.rietica.org).
[39] V. K. Pecharsky, J. O. Moorman, and K. A. Gschneidner, Jr., Rev. Sci. Instrum. **68**, 4196 (1997).
[40] V. I. Anisimov, F. Aryasetiawan, and A. I. Lichtenstein, J. Phys.: Condens. Matter **9**, 767 (1997).
[41] B. N. Harmon, V. P. Antropov, A. I. Lichtenstein, I. V. Solovyeb, and V. I. Anisimov, J. Phys. Chem. Solids **56**, 1521 (1995).
[42] O. K. Andersen and O. Jepsen, Phys. Rev. Lett. **53**, 2571 (1984).
[43] U. von Barth and L. Hedin, J. Phys. C **5**, 1629 (1972).
[44] F. Casanova, S. de Brion, A. Labarta, and J. Batlle, J. Phys. D **38**, 3343 (2005).
[45] C. Magen, P. A. Algarabel, L. Morellon, J. P. Araújo, C. Ritter, M. R. Ibarra, A. M. Pereira, and J. B. Sousa, Phys. Rev. Lett. **96**, 167201 (2006).
[46] Z. W. Ouyang, V. K. Pecharsky, K. A. Gschneidner, Jr., D. L. Schlagel, and T. A. Lograsso, Phys. Rev. B **74**, 094404 (2006).
[47] D. Paudyal, V. K. Pecharsky, K. A. Gschneidner, Jr., and B. N. Harmon, Phys. Rev. B **75**, 094427 (2007).
[48] V. Svitlyk, G. J. Miller, and Y. Mozharivskyj, J. Am. Chem. Soc. **131**, 2367 (2009).
[49] D. Paudyal, V. K. Pecharsky, K. A. Gschneidner, Jr., and B. N. Harmon, Phys. Rev. B **73**, 144406 (2006).
[50] L. Tan, A. Kreyssig, J. W. Kim, A. I. Goldman, R. J. McQueeney, D. Wermeille, B. Sieve, T. A. Lograsso, D. L. Schlagel, S. L. Budko, V. K. Pecharsky, and K. A. Gschneidner, Jr., Phys. Rev. B **71**, 214408 (2005).
[51] E. M. Levin, K. A. Gschneidner, Jr., T. A. Lograsso, D. L. Schlagel, and V. K. Pecharsky, Phys. Rev. B **69**, 144428 (2004).